A Concatenated Multitone Multiple-Antenna Air-Interface for the Asynchronous Multiple-Access Channel

Andrea M. Tonello, *Member, IEEE*

***Abstract*—In this paper, we present a novel transmission technology approach for application in the asynchronous multiple-access wireless channel (uplink). It is based on the concatenation of an inner filtered multitone (FMT) modulator with transmission over multiple antennas, and an outer space–time cyclically prefixed discrete multitone (ST-CP-DMT) modulator. The inner modulator is used to efficiently realize frequency-division multiplexing of the users by partitioning the FMT subchannels among them. The outer modulator copes with the residual subchannel intersymbol interference and it further implements a form of transmit diversity. Frequency and space diversity is exploited via direct sequence (DS) data spreading across the DMT tones. The design parameters are flexible and are chosen to make the proposed air-interface robust to the time and frequency offsets between uplink users, as well as to the channel time-frequency selectivity. Furthermore, the ST-CP-DMT modulator with DS spreading provides sensible performance gains. In particular, it yields a diversity gain for the users that transmit at low rate and occupy a fraction of the overall spectrum.**

***Index Terms*—Concatenated multitone modulation, discrete multitone (DMT) modulation, filtered multitone (FMT) modulation, multiple access, multiple transmit antennas, multiuser multiple-input–multiple-output (MIMO) systems, orthogonal frequency-division multiplexing (OFDM).**

I. Introduction

IN THIS PAPER, we present an air-interface for the asynchronous multiple-access channel (uplink) that combines concatenated multitone modulation with multiple-antenna transmission. It is intended for application in next-generation wireless scenarios [cellular or wireless local area network (WLAN)]. Currently, WLAN technology (IEEE 802.11a) deploys 20 MHz channels supporting data rates up to 54 Mbit/s, while third-generation (3G) cellular technology [Universal Mobile Telecommunications System (UMTS), code-division multiple-access (CDMA) 2000] deploys 5 MHz channels supporting data rates up to 2 Mbit/s (up to 10 Mbit/s in downlink high-speed-data recent releases). The gap in offered data rates between the two technologies is significant. Different available spectrum and mobility/coverage requirements in part justify it. Fourth-generation (4G) wireless systems shall be able to increase current cellular data rates to bridge the gap with WLAN technology. Recently, most of the work has focused on improvements for the forward link rather than the reverse link. This is justified by the general opinion that the traffic is asymmetric since most high-speed services are required in the downlink only, e.g., file downloading and voice/video streaming services. Indeed, the reverse link poses further challenges that are due to the asynchronous nature of this link. That is, the communication channels of distinct users can be considered independent and they experience propagation delays, carrier frequency offsets, Doppler from movement, and transmission power limitations. These impairments may translate into multiple-access interference (MAI) that severely affects performance. This is a well understood problem, e.g., in CDMA technology, that can be mitigated only with the use of complex multiuser receivers [1].

Among the various transmission technologies, multicarrier modulation has proven to be effective in simplifying the equalization task in severely dispersive fading channels [2]. In particular, orthogonal frequency-division multiplexing (OFDM) has been chosen in 802.11a together with a time-division multiple-access scheme. When multiplexing is done in a time-division fashion, the exploitation of the system resources may not exhibit sufficient granularity as required in multiuser bursty and heterogeneous traffic. A combination of both time-division and frequency-division multiplexing can show better utilization of the available resources [3]. Frequency-division multiplexing is obtained by partitioning the available OFDM tones among the active users. However, it should be noted that OFDM, referred to as discrete multitone (DMT) modulation in this paper, is severely affected by time misalignments and carrier frequency offsets that can be large in the reverse link. This is due to the fact that in conventional OFDM, subchannels exhibit a *sinc* like frequency response, therefore, their orthogonality can be easily lost in the absence of precise synchronization [4], [5]. In an asynchronous multiuser environment, increased robustness and better performance can be obtained with filtered multitone (FMT) modulation architectures where the subchannels are shaped with time-frequency concentrated pulses and are partitioned among the users [6]–[8]. The frequency concentrated subchannel pulses allow to avoid the intercarrier interference (ICI) and get low intersymbol interference (ISI) contributions [9], [10]. FMT modulation has the potentiality of achieving in fading channels better spectral efficiency than DMT modulation yet requiring

Manuscript received January 16, 2005; revised May 3, 2005. This work was supported in part by the Italian Ministry of Education, University, and Research (MIUR) under Project "Reconfigurable Platforms for Wideband Wireless Communications" prot. RBNE018RFY with the Fund for the Basic Research (FIRB). This work was presented in part at the IEEE ITG Workshop on Smart Antennas 2004, Munich, Germany, March 18–19, 2004.

The author is with the Dipartimento di Ingegneria Elettrica, Gestionale e Meccanica, Università di Udine, 33100 Udine, Italy (e-mail: tonello@uniud.it).

Digital Object Identifier 10.1109/JSAC.2005.862397

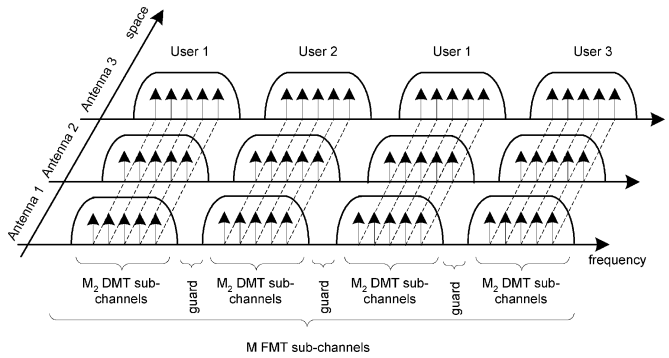

Fig. 1. Frequency-division multiplexing through inner FMT modulation concatenated with outer DMT modulation and transmission over multiple antennas.

sufficiently simple equalization [11], [12]. With uniformly spaced subcarriers and identical subchannel filters, an efficient digital implementation of an FMT modulator/demodulator is possible. As described in [10], it is based on a fast Fourier transform (FFT) and low rate subchannel filtering.

The novel scheme that we describe in this paper combines an inner FMT modulator with an outer, appropriately modified, cyclically prefixed DMT modulator with multiple-antenna transmission. The inner modulator is used to efficiently realize frequency-division multiplexing by partitioning the FMT subchannels among the users (Fig. 1). The outer modulator is used to cope with the residual ISI of the FMT subchannels and to provide a form of transmit diversity [13], [14]. It is here referred to as space–time cyclically prefixed DMT (ST-CP-DMT). Frequency and space diversity is exploited via direct sequence data spreading [15] across the DMT tones that fall within the FMT subchannels that are assigned to a given user. A description of the key elements of the proposed air interface is reported in Section II. The transmitter is described in Section III. In Section IV, we investigate the conditions under which the system orthogonalizes the asynchronous multiple-access channel. Considerations on the system design are given in Section V. In Section VI, a comprehensive set of numerical results is reported to show the robustness of the scheme, and to determine the performance gains that the transmit diversity scheme provides. A comparison with multiuser DMT and multicarrier CDMA (MC-CDMA) employing OFDM [15], [16] is also made. Finally, the conclusions follow. In Table I, we summarize acronyms and notation.

TABLE I
ACRONYMS AND NOTATION

DMT	Discrete multitone modulation (OFDM)
FMT	Filtered multitone modulation
ST-CP-DMT	Space-time cyclically prefixed discrete multitone modulation
N_T	Number of transmit antennas
N_R	Number of receive antennas
N_U	Number of users
M	Number of tones of inner FMT modulator
M_u	Number of FMT sub-channels assigned to user u
T	Transmission period
$W=1/T$	Nominal overall system bandwidth
$g(nT)$	Prototype pulse of FMT modulator
$f_k-f_{k-1}=1/(MT)$	FMT sub-carrier spacing
$T_0=NT=MT(1+\alpha)$	FMT sub-channel symbol period with $\alpha \geq 0$
$\Delta_f^{(u)}$	Carrier frequency offset of user u
$\Delta_\tau^{(u)}$	Time offset of user u
M_2	Number of tones of outer ST-CP-DMT modulator
$N_2=M_2+\mu$	$\mu \geq 0$ cyclic prefix outer ST-CP-DMT modulator
$T_2=N_2T_0$	ST-CP-DMT sub-channel symbol period

II. Proposed Concatenated Multitone Multiuser Approach

In the uplink air-interface that we describe in this paper, the users are multiplexed in a frequency-division fashion (Fig. 1) through the serial concatenation of two multitone modulators. As shown in Fig. 2, the transmitter of each user comprises three stages: first a direct sequence (DS) data spreading stage, then a cyclically prefixed DMT modulator, and finally, an inner (with respect to the physical media) FMT modulation stage with transmission over N_T antennas. The inner discrete-time FMT modulator is deployed for users' channelization, i.e., to split the available spectrum into slices that are assigned to distinct users. A user in a cell/sector can be assigned with one or more of the M FMT subchannels according to his/hers data rate requirement. The N_T antenna signals of a given user are simultaneously transmitted and occupy the spectrum corresponding to the assigned FMT subchannels (Fig. 1). Each FMT subchannel is shaped with a filter having frequency concentrated response, e.g., root-raised-cosine pulse. An appropriate frequency guard can be set in order to enhance the frequency separation of the FMT subchannels. With ideal band limited pulses the presence of time misalignments across users or channel time dispersion does not compromise the orthogonality between the users' signals. The frequency guards yield protection against the carrier frequency offsets that may exist between users [6], although at the expense of data rate. In our design the number of FMT subchannels may not be large enough to obtain a perfectly flat subchannel frequency response. Hence, some residual ISI arises. The outer cyclically prefixed DMT modulator uses M_2 tones and is applied serially on each FMT subchannel to cope with the residual ISI. This allows to use a simple FFT-based receiver with one-tap equalization per FMT subchannel.

It should be noted that the low-rate users that are assigned with a small number of FMT subchannels do not take advantage of the full frequency diversity that is provided by the broadband fading channel. In this case, the use of multiple-antenna transmission is an effective mean to increase performance [17]. In particular, in this paper, we consider a transmit diversity scheme that we refer to as space–time cyclically prefixed DMT (ST-CP-DMT) modulation. The ST-CP-DMT modulator sends cyclically shifted replicas of the data blocks over the antennas [13], [14] without increasing the channel time dispersion as in other transmit delay diversity schemes [19], [20]. In our system, the ST-CP-DMT modulator is applied serially over each FMT subchannel. It orthogonalizes the N_T spatial channels for any number of transmit antennas without decreasing the transmission rate. This allows to use a conventional FFT-based DMT receiver differently from other DMT (OFDM) space–time coded systems [21], [22] that require joint detection of the N_T transmitted signals. To exploit space and frequency diversity,

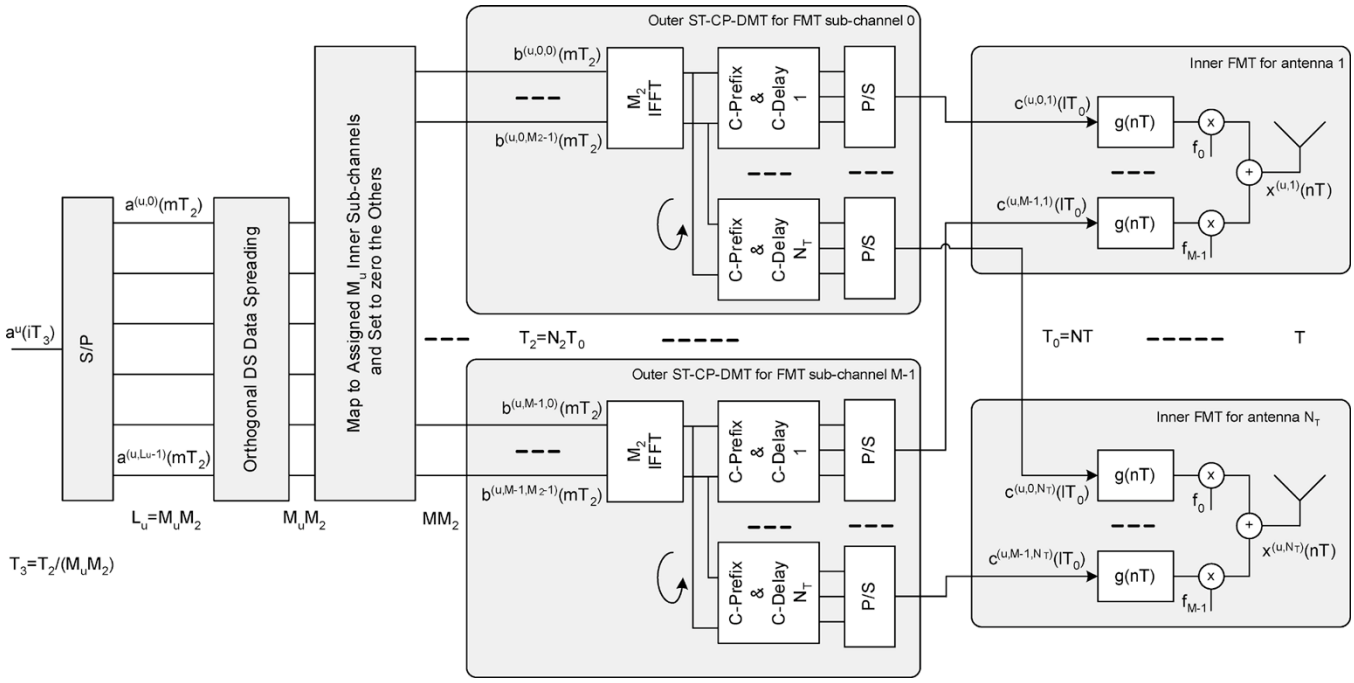

Fig. 2. Transmitter of user u.

we use direct sequence (DS) data spreading across the DMT tones that fall within the FMT subchannels that are assigned to a given user. DS spreading does not decrease the transmission rate [15]. Further, the detection complexity is small when it is performed with a zero-forcing (ZF) or minimum mean-square error (MMSE) approach, as it is considered in this paper.

III. Transmission Architecture

In this section, we describe the proposed transmission architecture. The transmitter (Fig. 2) of a given user comprises an inner FMT modulator (described in Section III-A), an outer ST-CP-DMT modulator (described in Section III-B), and finally, a DS data spreading stage (described in Section III-C). We use this order because the transmitter is modular and can work in principle with the inner FMT modulator only.

A. Inner FMT Modulator, User Multiplexing, and Multiple Transmit Antennas

We assume to frequency multiplex N_U uplink users. Each user has an FMT modulated-based transmitter that is equipped with N_T transmit antennas. Multiplexing is realized by partitioning the M overall FMT subchannels among the users [6], [7]. Each FMT subchannel is shaped with the real prototype pulse $g(nT)$ that has frequency concentrated response. The FMT subchannels are centered at frequency f_k, $k = 0, \ldots, M-1$, with separation $f_k - f_{k-1} = 1/(MT)$, where $W = 1/T$ equals the overall transmission bandwidth. T is assumed as the time unit in the following. The subchannel symbol period is $T_0 = NT = MT(1+\alpha)$, which corresponds to a noncritically sampled FMT architecture [9] for $\alpha > 0$. The choice of the parameters is flexible. For instance, with an ideal root-raised-cosine prototype pulse with roll-off α_1, we can choose $\alpha = \alpha_1 + \alpha_2$ with $\alpha_2 > 0$ such that a frequency guard equal to α_2/T_0 exists between adjacent subchannels.

The N_T antenna signals of a given user are simultaneously transmitted and occupy the spectrum corresponding to the assigned FMT subchannels (Fig. 1). The low-pass discrete-time signal that is transmitted by user u on antenna t can be written as

$$x^{(u,t)}(nT) = \sum_{k=0}^{M-1} \sum_{l \in \mathbb{Z}} c^{(u,k,t)}(lT_0) g(nT - lT_0) e^{j2\pi f_k nT}$$
$$f_k = \frac{k}{(MT)} \quad (1)$$

$c^{(u,k,t)}(lT_0)$ denotes the complex symbol that is transmitted at time instant lT_0 by user u over the FMT subchannel of index $k = 0, \ldots, M-1$ and antenna of index $t = 1, \ldots, N_T$. The symbols $c^{(u,k,t)}(lT_0)$ belong to the phase-shift keying/quadrature amplitude modulation (PSK/QAM) constellation unless the outer ST-CP-DMT modulator is used. In fact, in the latter case they are obtained by an outer DMT transform as explained in the next subsection. Distinct FMT subchannels can be assigned to distinct users. Thus, the symbols are set to zero for the unassigned FMT subchannels

$$c^{(u,k,t)}(lT_0) = 0 \text{ for } k \notin K_u \quad (2)$$

where K_u denotes the set of M_u subchannel indices that are assigned to user u. It should be noted that there is one FMT modulator per transmit antenna. Finally, the discrete time signal (1) is digital-to-analog converted before modulation at radio frequency.

B. Outer Space–Time Cyclically Prefixed DMT Modulator

The outer modulator is a modified DMT modulator with M_2 tones that is applied serially on each FMT subchannel (Fig. 2). It is here referred to as space–time cyclically prefixed DMT

(ST-CP-DMT). In [13], it is referred to as cyclic delay diversity. It realizes a form of transmit diversity and, in principle, it allows to obtain a flat frequency response for each FMT inner subchannel. As shown in Fig. 2, at the ST-CP-DMT modulator stage of user u and FMT subchannel k, we take a block of M_2 symbols that belong to the PSK/QAM constellation (unless DS data spreading is applied as described in the next section). The block of symbols is denoted as

$$b^{(u,k,k')}(mT_2) = b^{(u,k,k')}(mN_2T_0) \text{ for } k' = 0, \ldots, M_2 - 1. \tag{3}$$

Each block is transformed by an M_2-point inverse discrete Fourier transform (IDFT), or by its efficient implementation the inverse FFT (IFFT). A cyclic prefix of length $\mu \geq 0$ is added to generate an output block of N_2 symbols to cope with the channel time dispersion due to frequency selectivity. The block has transmission period $T_2 = N_2T_0$, with $N_2 = M_2 + \mu$. The block at the output of the IDFT is transmitted by an antenna after the insertion of a cyclic delay. In formulae, we generate N_T blocks of N_2 symbols each as follows:

$$\begin{aligned} &c^{(u,k,t)}(lT_0) \\ &\quad = c^{(u,k,t)}(nT_0 + mN_2T_0) \\ &\quad = \frac{1}{\sqrt{M_2N_T}} \sum_{k'=0}^{M_2-1} b^{(u,k,k')}(mT_2) e^{j(2\pi/M_2)(n-\mu-\delta^{(t)})k'} \end{aligned} \tag{4}$$

for $l = n + mN_2$, $n = 0, \ldots, N_2 - 1$, $m \in \mathbb{Z}$, and $t = 1, \ldots, N_T$. $\delta^{(t)}$ is an integer delay. Assuming for instance $\delta^{(t)} = t - 1$, the output of (4) can be collected in the matrix shown in (5) at the bottom of the page, where $c_n = (M_2N_T)^{-1/2} \sum_{k'=0}^{M_2-1} b^{(u,k,k')}(mT_2) e^{j2\pi nk'/M_2}$. The rows are transmitted by distinct antennas. The number of DMT tones, spaced by $1/(M_2T_0)$, fulfills the relation $M_2 > \mu + N_T$ with μT_0 larger, possibly, than the maximum FMT subchannel time dispersion. The cyclic prefix does not increase with the number of transmit antennas (Section IV-B). It should be noted that the symbol stream (4) is fed to the FMT modulator. In particular, the symbol stream $c^{(u,k,t)}(lT_0)$ of indices (u, k, t) belongs to user u, and it is transmitted on the FMT subchannel k of the tth antenna. According to (3), $b^{(u,k,k')}(mT_2)$ is the data symbol transmitted by user u over the DMT subchannel k' that falls within the FMT subchannel k. Essentially, the concatenation of the two modulators generates $L_u = M_uM_2$ narrow subchannels for user u, where $M_u \geq 1$ is the number of FMT subchannels that are assigned to user u. The ST-CP-DMT transform can be viewed as a rate one space–time block code, i.e., a transmit diversity scheme, such that the FMT subchannel k supports a net symbol rate of $M_2/(N_2T_0)$ symb/s. The goal of the ST-CP-DMT modulator is to increase the diversity resources (see Section IV-B), i.e., to transform spatial diversity into frequency diversity.

C. Direct Sequence Data Spreading

To exploit frequency and spatial diversity, we consider in this paper the deployment of DS data spreading [15] across the $L_u = M_uM_2$ narrow subchannels that are obtained via the concatenation of the two modulators of user u (Fig. 2). We assume Walsh–Hadamard spreading of length L_u although a shorter code can be used. Thus, starting from a block of L_u PSK/QAM data symbols $a^{(u,i)}(mT_2)$, $i = 0, \ldots, L_u - 1$, of user u, spreading yields

$$b^{(u,k,k')}(mT_2) = \frac{1}{\sqrt{L_u}} \sum_{i=0}^{L_u-1} a^{(u,i)}(mT_2) s\Big(i, k' + C^{(u)}(k)M_2\Big) \tag{6}$$

with $k' = 0, \ldots, M_2 - 1$, and $C^{(u)}(k) \in [0, \ldots, M_u - 1]$ for $k \in K_u$ is the inverse of the function that yields the indices of the FMT subchannels of user u. $s(i, n)$ are the elements of the nth column of the Walsh–Hadamard matrix of size L_u. The block $b^{(u,k,k')}(mT_2)$ is then fed to the ST-CP-DMT modulator (4). The procedure implements a form of space–frequency data spreading and it does not add redundancy, i.e., we keep the data rate equal to $M_2/(N_2T_0)$ symb/s per FMT subchannel such that user u has an overall transmission rate equal to $M_uM_2/(N_2T_0)$ that depends on M_u. Different users may have variable length codes that depend on M_u. Equal rate users can have the same spreading codes if they are assigned to distinct FMT channels. Although not considered in this paper, spreading can occur also across DMT blocks, i.e., along the temporal dimension.

IV. Asynchronous Multiple-Access Channel and Demodulation Stages

In the uplink, the signals of the N_U users propagate through independent time-variant frequency-selective fading channels. We assume an equivalent discrete-time low-pass channel model and a receiver that is equipped with N_R receive antennas. Thus, the received sample for receive antenna r at time instant $\tau_i = iT + \Delta_0$ (where $i \in \mathbb{Z}$ and Δ_0 is a sampling phase), can be written as shown in (7) and (8) at the bottom of the next page [6], where $w^{(r)}(\tau_i)$ is a sequence of independent identically distributed (i.i.d.) zero-mean Gaussian random variables, while (8) is the subchannel signal of index k that is transmitted by antenna t of user u [see also (1)]. In this model, $g_{\mathrm{CH}}^{(u,t,r)}(\tau_1; \tau_2)$ is the equivalent low-pass time-variant impulse response of the broadband channel for the tth transmit–rth receive antenna link of user u. It includes the effects of the filters in the digital-to-analog and

$$N_T \updownarrow \begin{bmatrix} c_{M_2-\mu} & \cdots & c_{M_2-1} & c_0 & c_1 & \cdots & c_{M_2-1} \\ c_{M_2-\mu-1} & \cdots & c_{M_2-2} & c_{M_2-1} & c_1 & \cdots & c_{M_2-2} \\ \cdots & \cdots & \cdots & \cdots & \cdots & \cdots & \cdots \\ c_{M_2-\mu-N_T+1} & \cdots & c_{M_2-N_T} & c_{M_2-N_T+1} & \cdots & \cdots & c_{M_2-N_T} \end{bmatrix} \tag{5}$$

$$\underbrace{\qquad\qquad\qquad\qquad\qquad\qquad\qquad}_{N_2}$$

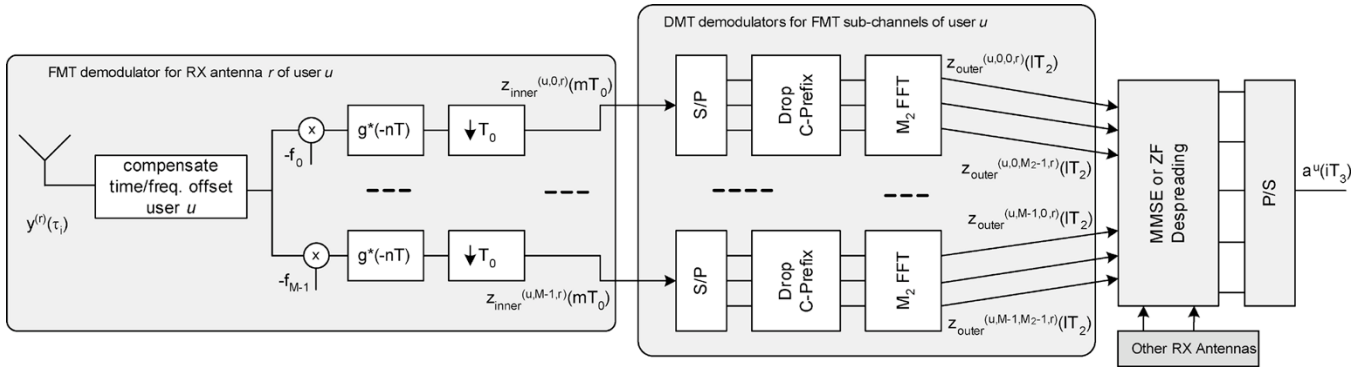

Fig. 3. Receiver of user u (the processing blocks for receive antenna r are shown).

the analog-to-digital converters at the transmitter and receiver sides. Furthermore, $\Delta_\tau^{(u,k,t,r)}$, $\Delta_f^{(u,k,t,r)}$, $\phi^{(u,k,t,r)}$ are, respectively, the time offset, the carrier frequency offset (assumed much smaller than $1/T$), and the phase offset of user u, FMT subchannel k, and antenna link (t,r). We assume the uplink users to have independent fading channels and time/frequency offsets.

As shown in Fig. 3, detection is accomplished on a user by user base with a three-stage receiver that first performs demodulation for the inner FMT modulator, then it runs ST-CP-DMT demodulation, and finally, it applies despreading and data decision. In the following treatment, we further assume the time/frequency/phase offsets to be identical for all transmit-receive antenna links and FMT subchannels that are assigned to a given user such that we can drop the dependency on the indices (k,t,r), e.g., $\Delta_\tau^{(u,k,t,r)} \rightarrow \Delta_\tau^{(u)}$. This is realistic in practical scenarios and it simplifies the notation.

A. Inner FMT Demodulation Stage

In the FMT demodulation stage, we first acquire time/frequency synchronization with each active user. Then, for each user, we run FMT demodulation via a bank of filters that is matched to the transmitter bank, and we sample the outputs at rate $1/T_0$. Assuming knowledge of the time and frequency offsets (that have in practice to be estimated [23]), the sequence of samples at the front-end filter output of FMT subchannel $\tilde{k}$ of user $\tilde{u}$ and receive antenna r that compensates the time offset $\Delta_\tau^{(\tilde{u})}$, and the frequency offset $\Delta_f^{(\tilde{u})}$ of only user $\tilde{u}$, can be written as shown in (9) and (10) at the bottom of the page, where $\eta^{(\tilde{u},\tilde{k},r)}(mT_0)$ is the sequence of filtered noise samples, $\phi^{(u),(\tilde{u})} = \phi^{(u)} + 2\pi\Delta_f^{(u)}\Delta_\tau^{(\tilde{u})}$ is a phase term, and $g_{EQ}^{(u,k,t),(\tilde{u},\tilde{k},r)}(lT_0;mT_0)$ is the multichannel time-variant impulse response between the input subchannel of indices

$$y^{(r)}(\tau_i) = \sum_{u=1}^{N_U}\sum_{t=1}^{N_T}\sum_{k=0}^{M-1}\sum_{n\in\mathbb{Z}} x^{(u,k,t)}(nT)\, g_{\mathrm{CH}}^{(u,t,r)}(\tau_i - nT - \Delta_\tau^{(u,k,t,r)};\tau_i)\, e^{j\left(2\pi\Delta_f^{(u,k,t,r)}\tau_i + \phi^{(u,k,t,r)}\right)} + w^{(r)}(\tau_i) \tag{7}$$

$$x^{(u,k,t)}(nT) = \sum_{l\in\mathbb{Z}} c^{(u,k,t)}(lT_0)\, g(nT - lT_0)\, e^{j2\pi f_k nT} \tag{8}$$

$$\begin{aligned} z_{\mathrm{inner}}^{(\tilde{u},\tilde{k},r)}(mT_0) &= \sum_{i\in\mathbb{Z}} y^{(r)}(iT + \Delta_\tau^{(\tilde{u})})\, g^*(iT - mT_0)\, e^{-j2\pi\left(f_{\tilde{k}} + \Delta_f^{(\tilde{u})}\right)iT} \\ &= \sum_{u=1}^{N_U}\sum_{t=1}^{N_T}\sum_{k=0}^{M-1}\sum_{l\in\mathbb{Z}} c^{(u,k,t)}(lT_0)\, g_{EQ}^{(u,k,t),(\tilde{u},\tilde{k},r)}(mT_0 - lT_0;mT_0) + \eta^{(\tilde{u},\tilde{k},r)}(mT_0) \end{aligned} \tag{9}$$

$$\begin{aligned} g_{EQ}^{(u,k,t),(\tilde{u},\tilde{k},r)}(lT_0;mT_0) = &\sum_{n\in\mathbb{Z}}\sum_{i\in\mathbb{Z}} g(nT + lT_0 - mT_0)\, g^*(iT - mT_0)\, e^{j2\pi\left(f_k nT - f_{\tilde{k}} iT + \Delta_f^{(u)} iT - \Delta_f^{(\tilde{u})} iT\right) + j\phi^{(u),(\tilde{u})}} \\ &\times g_{\mathrm{CH}}^{(u,t,r)}(iT - nT - \Delta_\tau^{(u)} + \Delta_\tau^{(\tilde{u})};iT + \Delta_\tau^{(\tilde{u})}) \end{aligned} \tag{10}$$

(u,k,t) and the output subchannel of indices $(\tilde{u},\tilde{k},r)$. We can rewrite (9) as follows:

$$\begin{aligned} z_{\text{inner}}^{(\tilde{u},\tilde{k},r)}(mT_0) &= \sum_{t=1}^{N_T}\sum_{l\in\mathbb{Z}} c^{(\tilde{u},\tilde{k},t)}(lT_0) g_{EQ}^{(\tilde{u},\tilde{k},t),(\tilde{u},\tilde{k},r)}(mT_0 - lT_0; mT_0) \\ &\quad + \text{ICI}^{(\tilde{u},\tilde{k},r)}(mT_0) + \text{MAI}^{(\tilde{u},\tilde{k},r)}(mT_0) \\ &\quad + \eta^{(\tilde{u},\tilde{k},r)}(mT_0) \end{aligned} \tag{11}$$

such that we can highlight, in general, the fact that the subchannel filter output of index $\tilde{k}$ may suffer from ISI, ICI (from the subchannels of index $k \neq \tilde{k}$ that are assigned to user $\tilde{u}$), and MAI (from all subchannels that belong to the other users) as a consequence of frequency overlapping subchannels, time/frequency offsets, and channel time/frequency selectivity.

To proceed, we model the channel with a T-spaced tap delay line that is time-invariant over the duration of the prototype pulse $g(nT)$ whose support is $S = [-N_gT, N_gT]$, and whose main lobe has duration approximately equal to T_0, i.e.,

$$\begin{aligned} &g_{\text{CH}}^{(u,t,r)}(iT - \Delta_\tau^{(u)} + \Delta_\tau^{(\tilde{u})}; iT + \Delta_\tau^{(\tilde{u})}) = \\ &\quad = \sum_{p\in P} \alpha_p^{(u,t,r)}(mT_0)\delta(iT - pT - \tau^{(u)}T + \tau^{(\tilde{u})}T) \\ &\quad \text{for } iT \in S + mT_0 \end{aligned} \tag{12}$$

where $\alpha_p^{(u,t,r)}(mT_0)$ are the channel tap amplitudes, P is the set of integer tap delays, and $\Delta_\tau^{(u)} = \tau^{(u)}T + \varepsilon^{(u)}$ for $\tau^{(u)} \in \mathbb{Z}$ and $0 \leq \varepsilon^{(u)} < T$. The fractional user delay is included in the tap delay line model. It follows that (10) can be written as shown in (13) at the bottom of the page, with $\hat{\phi}^{(u,k),(\tilde{u})} = \phi^{(u),(\tilde{u})} + 2\pi f_k T(\tau^{(\tilde{u})} - \tau^{(u)})$. Using the Parseval theorem, it can be shown that the multichannel impulse response (13) differs from zero only for $k = \tilde{k}$ if the following conditions hold true:

C1)

$$G(f) = 0 \text{ for } \frac{1+\alpha_1}{2T_0} \leq |f| \leq \frac{1}{2T}$$

C2)

$$|\Delta_f^{(u)}| \leq \frac{\alpha_2}{2T_0} \text{ for all } u$$

where $G(f)$ is the Fourier transform of the prototype pulse (assumed to be real). In other words, if the prototype pulse has a confined frequency response and the carrier frequency offsets of the users are smaller than half the frequency guard, the FMT subchannels do not overlap (despite the frequency shift) such that we do not get any ICI at the filter bank output. In this case that can be met with the appropriate system design, see Section V, (11) reads as shown in (14) at the bottom of the page. Thus, MAI is present only if the same FMT subchannel is assigned to more than one user. If we further assume to assign distinct FMT tones to distinct users, (14) becomes

$$\begin{aligned} z_{\text{inner}}^{(\tilde{u},\tilde{k},r)}(mT_0) &= \sum_{t=1}^{N_T}\sum_{q=-N_{Q1}}^{N_{Q2}} \beta_q^{(\tilde{u},\tilde{k},t,r)}(mT_0) c^{(\tilde{u},\tilde{k},t)}(mT_0 - qT_0) \\ &\quad + \eta^{(\tilde{u},\tilde{k},r)}(mT_0) \end{aligned} \tag{15}$$

$$\begin{aligned} \beta_q^{(\tilde{u},\tilde{k},t,r)}(mT_0) &= \sum_{p\in P} \alpha_p^{(\tilde{u},t,r)}(mT_0)\kappa_g(qT_0 - pT) e^{-j(2\pi/M)p\tilde{k} + j\phi^{(\tilde{u}),(\tilde{u})}} \end{aligned} \tag{16}$$

where $\kappa_g(mT) = \sum_i g(iT)g^*(iT - mT)$ is the prototype pulse autocorrelation, and $N_QT_0 = (N_{Q1} + N_{Q2} + 1)T_0$ is the duration of the T_0-spaced subchannel with taps $\beta_q^{(\tilde{u},\tilde{k},t,r)}(mT_0)$. N_Q depends on the channel delay spread, the prototype pulse, and the number of FMT tones, but, practically, it can be considered small. Therefore, at the receiver, the FMT subchannel $\tilde{k}$ of user $\tilde{u}$ sees ISI and the superposition of the signals that are simultaneously transmitted by the N_T antennas. If we do not use the outer ST-CP-DMT modulator, we need to accomplish data detection at this stage. Since there is ISI, subchannel space–time equalization is required [14], [24]. However, for the particular transmit diversity scheme that we consider in this paper the spatial channels are orthogonal, as we show in the next section and simple one tap equalization is required.

$$\begin{aligned} &g_{EQ}^{(u,k,t),(\tilde{u},\tilde{k},r)}(lT_0; mT_0) \\ &\quad = \sum_{p\in P} \alpha_p^{(u,t,r)}(mT_0) \\ &\quad \times \sum_{i\in\mathbb{Z}} e^{j2\pi\left(f_kiT - f_kpT - f_{\tilde{k}}iT + \Delta_f^{(u)}iT - \Delta_f^{(\tilde{u})}iT\right) + j\hat{\phi}^{(u,k),(\tilde{u})}} g(iT - pT - \tau^{(u)}T + \tau^{(\tilde{u})}T + lT_0 - mT_0)g^*(iT - mT_0) \end{aligned} \tag{13}$$

$$z_{\text{inner}}^{(\tilde{u},\tilde{k},r)}(mT_0) = \sum_{u=1}^{N_U}\sum_{t=1}^{N_T}\sum_{l\in\mathbb{Z}} c^{(u,\tilde{k},t)}(lT_0) g_{EQ}^{(u,\tilde{k},t),(\tilde{u},\tilde{k},r)}(mT_0 - lT_0; mT_0) + \eta^{(\tilde{u},\tilde{k},r)}(mT_0). \tag{14}$$

B. Outer ST-CP-DMT Demodulation and Data Despreading

Let us start from (15) and let us collect the FMT front-end output samples of receive antenna r and subchannel $\tilde{k}$, into blocks of N_2 samples that we denote as $z_{\text{inner}}^{(\tilde{u},\tilde{k},r)}(nT_0 + lN_2T_0)$ for $l \in \mathbb{Z}$, $n = 0, \ldots, N_2-1$. Now, for each receive antenna and FMT subchannel, ST-CP-DMT demodulation (Fig. 3) is accomplished by dropping the cyclic prefix in the block $z_{\text{inner}}^{(\tilde{u},\tilde{k},r)}(nT_0 + lT_2)$ and applying an M_2-point DFT. Then, under the following conditions:

- C3) μT_0 larger than the FMT subchannel time dispersion $(N_Q - 1)T_0$;
- C4) time-invariant channel in a window of duration $T_2 = N_2T_0$;

the DFT output of index $k' = 0, \ldots, M_2 - 1$ reads [1]

$$z_{\text{outer}}^{(\tilde{u},\tilde{k},k',r)}(lT_2) = H^{(\tilde{u},\tilde{k},k',r)}(lT_2)b^{(\tilde{u},\tilde{k},k')}(lT_2) + n^{(\tilde{u},\tilde{k},k',r)}(lT_2) \tag{17}$$

$$H^{(\tilde{u},\tilde{k},k',r)}(lT_2) = \frac{1}{\sqrt{N_T}} \sum_{t=1}^{N_T} \sum_{q=0}^{N_Q} \beta_q^{(\tilde{u},\tilde{k},t,r)}(lT_2) e^{-j(2\pi/M_2)(q+\delta^{(t)})k'}. \tag{18}$$

According to (17), the DFT output of index k' is equal to the superposition of a noise contribution with the data symbol $b^{(\tilde{u},\tilde{k},k')}(lT_2)$. The data symbol is weighted by an equivalent channel transfer function $H^{(\tilde{u},\tilde{k},k',r)}(lT_2)$ that is obtained by a transform of the fading channel responses of all antennas that we assume to be statistically independent. Therefore, each DFT output sees a single-input–single-output flat faded channel, i.e., the multiple transmit antenna system is transformed into a single transmit antenna system, where the spatial diversity translates into increased frequency diversity [18]. If the symbols $b^{(\tilde{u},\tilde{k},k')}(lT_2)$ belong to the PSK/QAM constellation, data decisions are made after maximal ratio combining of the N_R received signals (17). However, when DS data spreading is used the output of the ST-CP-DMT demodulator reads [substituting (6) in (17)]

$$z_{\text{outer}}^{(\tilde{u},\tilde{k},k',r)}(lT_2) = \frac{H^{(\tilde{u},\tilde{k},k',r)}(lT_2)}{\sqrt{L_u}} \times \sum_{i=0}^{L_u-1} a^{(\tilde{u},i)}(lT_2) s\left(i, k' + C^{(\tilde{u})}(\tilde{k})M_2\right) + n^{(\tilde{u},\tilde{k},k',r)}(lT_2). \tag{19}$$

Thus, from (19), we can accomplish despreading with either a zero-forcing (ZF) or an MMSE approach on a per subchannel basis [15], [25]. In the latter case, with N_R receive antennas, the decision metric for the ith data symbol $a^{(\tilde{u},i)}(lT_2)$ is generated as shown in (20) at the bottom of the page, where σ_η^2 is the variance of the noise. With ZF detection under the conditions C1-C4, we perfectly equalize the channel, i.e., we get the PSK/QAM data symbols $a^{(\tilde{u},i)}(lT_2)$, $i = 0, \ldots, L_u - 1$. However, MMSE performs better because of the noise enhancements of ZF detection.

The ST-CP-DMT modulator allows to increase the diversity resources that can be limited when a small number of FMT subchannels are assigned to a user. It should be noted that without channel coding or DS data spreading no diversity exploitation is possible since the concatenation of the outer and inner modulators generates, for user u, M_2M_u nonoverlapping flat faded channels.

C. Remarks

We point out that if the conditions C1-C4 that led to (20) do not hold true, some interference components can be present. In particular, C1-C2 grant the absence of ICI and MAI at the output of the FMT receiver filter bank. The interference at the FMT front-end output propagates to the output of the ST-CP-DMT demodulator. Furthermore, when C3-C4 do not hold true, the DFT output experiences ICI and ISI. In conclusion, if for simplicity we assume ZF detection, (20) can be manipulated to obtain $z_{\text{despr}}^{(\tilde{u},i)}(lT_2) = a^{(\tilde{u},i)}(lT_2) + \text{ISI} + \text{ICI} + \text{MAI} + \text{noise}$. However, the evaluation of the signal-to-inference power ratio shows that it is high with the appropriate system design as described below. In this paper (Section VI), we report a comprehensive set of simulation results to assess the performance in terms of bit-error rate (BER) for various channel conditions.

V. System Design and Example of System Parameters

The design of the system has the goal of orthogonalizing the asynchronous multiple-access channel that exhibits time/frequency offsets and channel time/frequency selectivity. The

[1] This can be easily proved by observing that under conditions C2-C4, (15) reads for the samples of index $n = \{\mu - N_{Q1}, \ldots, N_2 - N_{Q1} - 1\}$ (neglecting the noise term)

$$z_{\text{inner}}^{(\tilde{u},\tilde{k},r)}(nT_0 + lN_2T_0) = (M_2N_T)^{-1/2} \sum_{t=1}^{N_T} \sum_{q=-N_{Q1}}^{N_{Q2}} \sum_{k'=0}^{M_2-1} \beta_q^{(\tilde{u},\tilde{k},t,r)}(lT_2) \times b^{(\tilde{u},\tilde{k},k')}(lT_2) e^{j2\pi(n-\mu-\delta^{(t)}-q)k'/M_2}.$$

Thus, applying an M_2-point DFT (normalized by $\sqrt{M_2}$) on the block that starts with index $n = \mu - N_{Q1}$, we obtain (17)–(18).

$$z_{despr}^{(\tilde{u},i)}(lT_2) = \frac{1}{\sqrt{L_u}} \sum_{\tilde{k} \in K_u} \sum_{k'=0}^{M_2-1} \frac{\sum_{r=1}^{N_R} z_{\text{outer}}^{(\tilde{u},\tilde{k},k',r)}(lT_2) H^{(\tilde{u},\tilde{k},k',r)}(lT_2)^*}{\sum_{r=1}^{N_R} |H^{(\tilde{u},\tilde{k},k',r)}(lT_2)|^2 + \sigma_\eta^2} s^*\left(i, k' + C^{(\tilde{u})}(\tilde{k})M_2\right) \tag{20}$$

TABLE II
EXAMPLE OF SYSTEM PARAMETERS

4-PSK	Modulation
Walsh Hadamard	Spreading
$M = 32$	Number of tones of inner FMT modulator
$N_U = 32$	Maximum number of users per frame
$\alpha = \alpha_1 + \alpha_2 = 0.2 + 0.05$	Roll-off root-cosine pulse + guard factor in FMT
$T_0 = 40T$	FMT sub-channel symbol period
$R_{TOT\text{-}IN} = M/T_0 = 0.8/T$	Aggregate symbol rate (in symb/s) with FMT only
$M_2 = 32$	Number of tones outer ST-CP-DMT modulator
$\mu = 8$	Cyclic prefix length
$T_0(M_2+\mu) = 40T_0$	ST-CP-DMT sub-channel symbol period
$R_{TOT\text{-}OUT} = MM_2/(40T_0) = 0.64/T$	Aggregate rate (in symb/s) with outer modulator

number of FMT subcarriers is chosen such that a good trade off in terms of large coherence bandwidth $B_{\rm ch} \sim 1/\sigma_\tau$ and coherence time $T_{\rm ch} \sim 1/f_D$ with respect to the transmission parameters is safely fulfilled (σ_τ and f_D denote the delay spread and the maximum Doppler spread [27]). In turn, these are a function of the application scenario, i.e., mobility and coverage requirements. With a fixed transmission bandwidth $W = 1/T$, if we increase the number of FMT subchannels M, we can multiplex a larger number of users, and we can decrease the subchannel bandwidth. This adds more robustness to channel frequency selectivity at the expense of higher sensitivity to channel time selectivity since we obtain a longer subchannel symbol period T_0, and consequently, a longer DMT symbol duration which should be shorter than $T_{\rm ch}$ to fulfill the condition C4.

As an example, we report in Table II some parameters that we have used to assess the system performance. An important issue is the design of the prototype pulse that has to exhibit a frequency concentrated response. In this paper, we consider a truncated root-raised-cosine pulse with roll off $\alpha_1 = 0.2$ and duration $29T_0$, which yields a good separation among subchannels. We choose $M = 32$ for the inner FMT modulator and $M_2 = 32$ for the outer ST-CP-DMT modulator. A frequency guard $\alpha_2/T_0 = 0.05/T_0 = 0.04/(MT)$ between adjacent FMT subchannels is added such that the subcarrier spacing is $1/(MT) = (1+\alpha_1+\alpha_2)/T_0 = 1.25/T_0$ with $T_0 = 40T$. A cyclic prefix of duration $\mu T_0 = 8T_0$ is used at the DMT stage to cope with the subchannel residual ISI. Transmission is performed across distinct tones supporting up to 32 users. The minimum burst duration is $T_2 = 40T_0$ (DMT symbol duration). To increase the flexibility, the MAC layer may support both frequency and time-division multiplexing. That is, each inner subchannel can be shared in a time-division mode every MAC frame that comprises a certain number of bursts. With these parameters, if, we assume a transmission bandwidth of $1/T = 10$ MHz, the FMT subchannel bandwidth equals 312.5 kHz, the frequency guard equals 12.5 kHz, the cyclic prefix has duration 32 μs, and the DMT symbol duration is 0.16 ms. This allows to have perfect orthogonality at the DMT stage if the subchannel is shorter than the CP, and it is time invariant for 0.16 ms (Doppler in the order of 100 Hz if, we assume $T_{\rm ch} = 1/(5f_D)$, see Section VI-C). The minimum data rate (with single FMT subchannel) is $M_2/(N_2T_0) = 200$ ksymb/s/user while the aggregate rate is 6.4 Msymb/s (12.8 Mbit/s with 4-PSK).

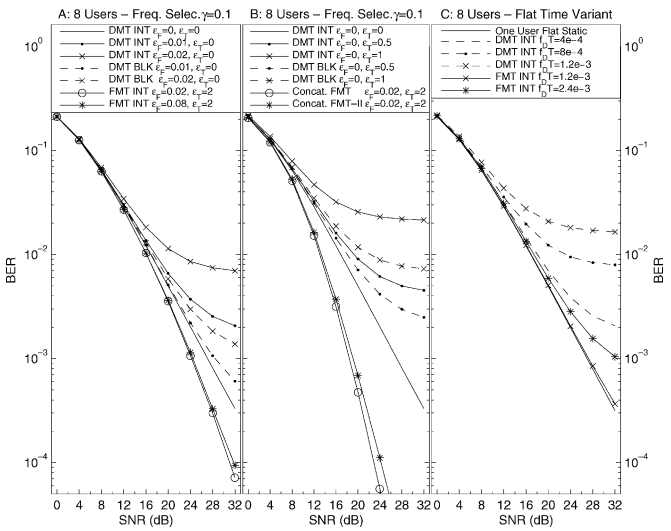

Fig. 4. Average BER performance of multiuser DMT, multiuser FMT, and concatenated DMT-FMT with eight full rate users with one transmit-receive antenna. Plot A-B: Frequency-selective fading with decay factor $\gamma = 0.1$, asynchronous users with $\Delta_{\tau,\max} = \varepsilon_T T_0$, $\Delta_{f,\max} = \varepsilon_F/(MT)$ with $M = 32$. Plot C: Synchronous users in fast flat fading with normalized Doppler $f_D T$.

Finally, we point out that the scheme is rather insensitive to the users' time offsets (with good subchannel separation), thus, it is not necessary to adjust their timing such that it is the same at the base station [26]. However, if timing is adjusted according to the downlink frame, the users' signals have a time offset (relatively to the base station reference) that is equal to the two-way propagation delay.

VI. SYSTEM PERFORMANCE

The performance of the proposed concatenated multitone multiple-antenna scheme is evaluated via simulations. We report BER as a function of the average symbol-energy-to-noise ratio (SNR). We assume the parameters in Table II with a truncated root-raised-cosine prototype pulse for the FMT modulator as described in Section V. The simulation assumes T has the time unit. In the proposed architecture, distinct users and antenna links have independent channels. Further, the users have independent uniformly distributed time offsets in $[0, \Delta_{\tau,\max}]$, and carrier frequency offsets in $[-\Delta_{f,\max}, \Delta_{f,\max}]$, that are assumed to be constant over the transmission of a frame of several outer DMT symbols. The users deploy 4-PSK modulation and have equal average power and number of antennas. The system is fully loaded (all subchannels are used) with users having the same rate. The FMT subchannels are allocated in an interleaved fashion, i.e., user u is allocated to subchannels of indices $k = u + nN_U, u = 0, \ldots, N_U - 1, n = 0, \ldots, M/N_U - 1$. We assume perfect knowledge of the channel and ideal time/frequency synchronization when, we demodulate the desired user.

A. Performance of the Inner FMT Stage and Comparison With Multiuser DMT

Our architecture can work with only the inner FMT stage. In this case, it corresponds to a multiuser FMT system [7]. In Fig. 4, we compare the inner FMT stage with a multiuser CP-DMT scheme that uses 128 tones and a CP of length 32.

The two systems have identical data rate. Single transmit-receive antenna is used. Detection is single-user-based with one tap equalization for the DMT scheme and with MMSE linear equalization with 11 taps for the FMT scheme [23]. Eight full rate users are active and have uniformly distributed time offsets in $[0, \varepsilon_T]T_0$, and frequency offsets in $[-\varepsilon_F, \varepsilon_F]/(MT)$ with $M = 32$ (number of FMT subchannels). In the DMT scheme, the users are multiplexed by partitioning the 128 tones in a block (BLK) or in an interleaved (INT) fashion. In Fig. 4(a) and (b), we consider quasi-static frequency-selective Rayleigh fading according to the model (12) with rays spaced by T. The rays are independent and have an exponential power delay profile with average power $\Omega_p \sim e^{-pT/(\gamma T_0)}$ for a normalized decay factor $\gamma = 0.1$. The channel is truncated at -20 dB. The BER is averaged over all users.

Fig. 4 shows that multiuser DMT is severely affected by the MAI that is generated by the users' frequency offsets and by the time offsets (together with the channel dispersion) that exceed the CP length. With the block tone allocation DMT is more robust than with the interleaved allocation [4]. However, DMT performs always worse than the multiuser FMT scheme for all the cases herein considered. For the FMT scheme, there is no visible degradation due to the MAI if $\Delta_{f,\max} \leq 0.02/(MT)$ although we use truncated prototype pulses (see also the next section). While uncoded DMT with synchronous users performs essentially as 4-PSK in flat fading, the FMT subchannel equalizer yields a diversity gain by the exploitation of the subchannel frequency selectivity. We note that the presence of the transmit-receive filter bank and the subchannel equalizer makes, in general, the FMT architecture more complex than the DMT solution assuming an identical number of subchannels. If, for instance, LT_0 is the duration of the prototype pulse and all subchannels are assigned to a given user, the efficient polyphase implementation in [10] allows to realize the transmit-receive filter banks with a complexity in the order of $(M/N \log_2 M + L)/T$ complex multiplications per second. If we increase M, the equalizer length can be shortened since we obtain flatter subchannel frequency responses [12]. We also point out that the filtering operation in the FMT system introduces some delay that is, however, small with a sufficiently short duration prototype pulse as the one considered in this paper.

Now, although the inner FMT scheme allows to implement a robust multiple-access system, its performance can be improved by concatenating the outer DMT stage and adding DS spreading. The curve labeled with *Concat. FMT* in Fig. 4(b) shows that at $\mathrm{BER} = 10^{-4}$ the improvement is 8 dB compared with the use of only the inner FMT stage. This is due to the capability of the concatenated scheme to exploit the wideband channel diversity. We note that in this case the two systems have different data rate (respectively, $0.64/T$ symb/s, and $0.8/T$ symb/s) because the CP in the outer modulator adds some redundancy. It is clear that the parameters can be changed depending upon the specific application scenario. For instance, instead of using the parameters in Table II, the concatenated scheme has a spectral efficiency of about $0.8/T$ symb/s if we choose $M = 32$, $N = 34$, $\alpha_1 = 0.0625$, $\alpha_2 = 0$, and a CP of length $\mu = 6$. With these parameters the subchannels are less spaced apart, and the outer DMT has a shorter CP compared with the scheme in Table II. Nevertheless, this concatenated scheme [curve labeled with *Concat. FMT-II* in Fig. 4(b)] yields at $\mathrm{BER} = 10^{-4}$ about 6.5 dB improvement over the inner FMT scheme and about 12 dB over synchronous DMT with identical data rate. Further performance improvements can be realized with multiple transmit antennas, as shown in the next section. In terms of complexity, in the concatenated system here simulated the FFT-based one-tap MMSE detector has lower complexity than the linear equalizer that we use for the FMT system. However, the concatenated scheme adds some extra complexity at the transmitter compared with the use of only the inner FMT stage because of the DMT modulators.

In Fig. 4(c), we assume a flat fading channel with Jakes' Doppler spectrum and normalized Doppler equal to $f_D T$. The eight users are synchronous but have independent channels. To stress the system, we assume a large normalized Doppler from $f_D T = 4 \times 10^{-4}$ to 2.4×10^{-3}. The curves show that fast fading introduces an error floor in the DMT curves because of the loss of the tones orthogonality [27]. On the contrary, the inner FMT stage is more robust to fast fading. This is because, (assuming ideal pulses) no intercarrier interference arises if f_D does not exceed half the frequency guard. However, fast fading can increase the subchannel ISI since it distorts the transmitted pulse.

B. Performance of the Concatenated DMT-FMT Architecture With Multiple Antennas

In this section, we report performance for the proposed concatenated architecture (with the parameters in Table II) when we use multiple transmit-receive antennas. The SNR is evaluated at the DMT receiver output. The cyclic delay for antenna t is set equal to $\delta^{(t)} = t - 1$. Spreading is accomplished with Walsh–Hadamard codes of length $M_2 M/N_U$ across the tones of the outer DMT modulator. In particular, with one user we can assign all FMT/DMT tones to him/her and spreading has, therefore, length 1024. With 32 users, all users have a single FMT subchannel, such that spreading has length 32. One tap MMSE detection at the output of the ST-CP-DMT demodulator stage according to (20) is used.

In Figs. 5 and 6, we show the BER as a function of the number of users and transmit antennas assuming a single receive antenna. The channel is frequency selective. As a reference, we plot also the performance of a single-user system in quasi-static flat fading that essentially corresponds to the BER of 4-PSK modulation in flat fading with single transmit-receive antenna (curve labeled with *one user flat*). The users are asynchronous with uniformly distributed time offsets in $[0, 2T_0]$, and frequency offsets in $[-0.02, 0.02]/(MT)$. Now, with a single transmit antenna [Fig. 5(a)] the only source of diversity comes from the media frequency selectivity. Here, the decay factor γ is set equal to 0.05. In this case, the performance decreases as the number of users increases because, in our fully loaded system, the number of FMT subchannels per user decreases and consequently each user cannot exploit the full broadband channel diversity. The performance is always better than the single-user flat fading scenario, which shows both the capability of the proposed scheme to exploit diversity and to be robust to the presence of time/frequency offsets across uplink users. The improvement as the number of transmit antennas

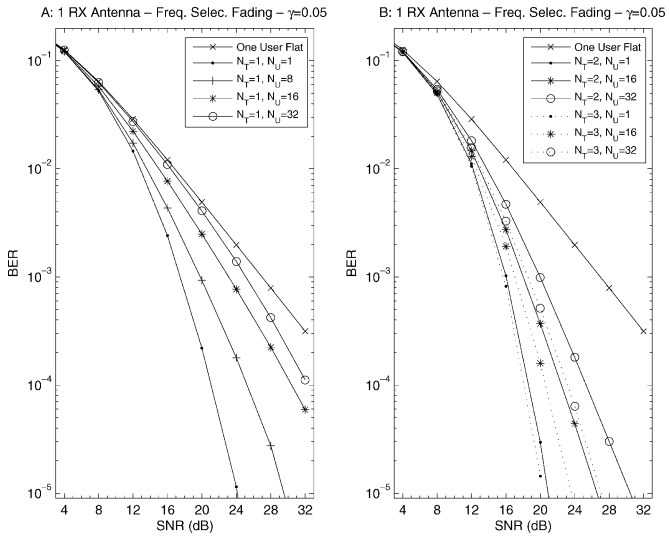

Fig. 5. Average BER performance of concatenated DMT-FMT for different number of users in a fully loaded system with one receive antenna in frequency-selective fading with decay factor $\gamma = 0.05$. Asynchronous users with $\Delta_{\tau,\max} = 2T_0$ and $\Delta_{f,\max} = 0.02/(MT)$. Plot A: One transmit antenna. Plot B: Two and three transmit antennas.

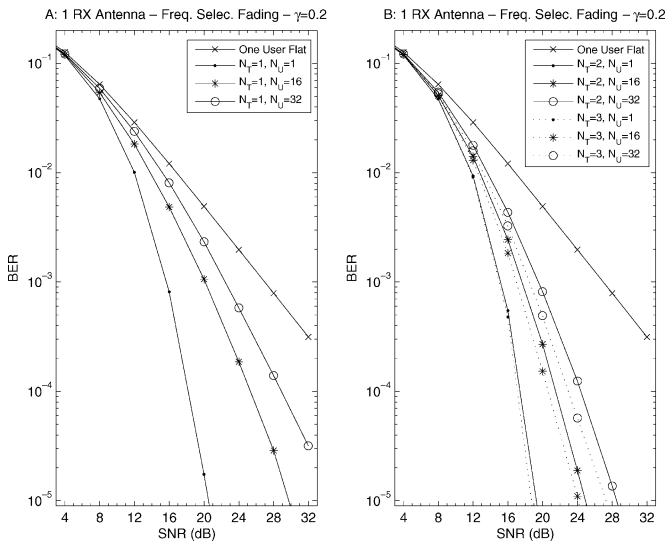

Fig. 6. Average BER performance of concatenated DMT-FMT for different number of users in a fully loaded system with one receive antenna in frequency-selective fading with decay factor $\gamma = 0.2$. Asynchronous users with $\Delta_{\tau,\max} = 2T_0$ and $\Delta_{f,\max} = 0.02/(MT)$. Plot A: One transmit antenna. Plot B: Two and three transmit antennas.

increases is significant, as shown in Fig. 5(b), especially when we multiplex a high number of users. At $\mathrm{BER} = 10^{-3}$, the gain for the 32 users case is 5 and 6.5 dB, respectively, with two and three antennas compared with the single-antenna case. When the channel frequency selectivity increases the gain provided by the transmit diversity scheme is still high although it incrementally diminishes, as shown in Fig. 6(a) and (b), where $\gamma = 0.2$.

When the users have a maximum frequency offset smaller than the frequency guard, we have not noticed any significant degradation due to the MAI that potentially can be generated by adjacent (independent) FMT subchannels. The degradation

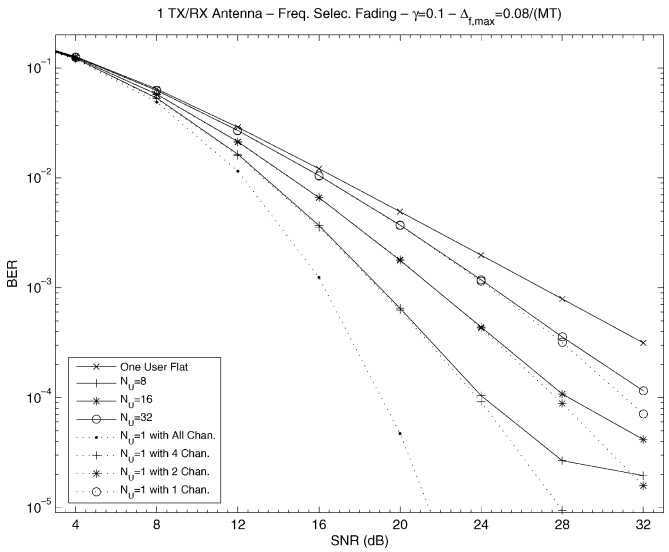

Fig. 7. Average BER performance of concatenated DMT-FMT with one transmit and one receive antenna in frequency-selective fading with decay factor $\gamma = 0.1$. Solid lines: Asynchronous users with $\Delta_{\tau,\max} = 2T_0$ and $\Delta_{f,\max} = 0.08/(MT)$. Dashed lines: One user with different number of assigned subchannels.

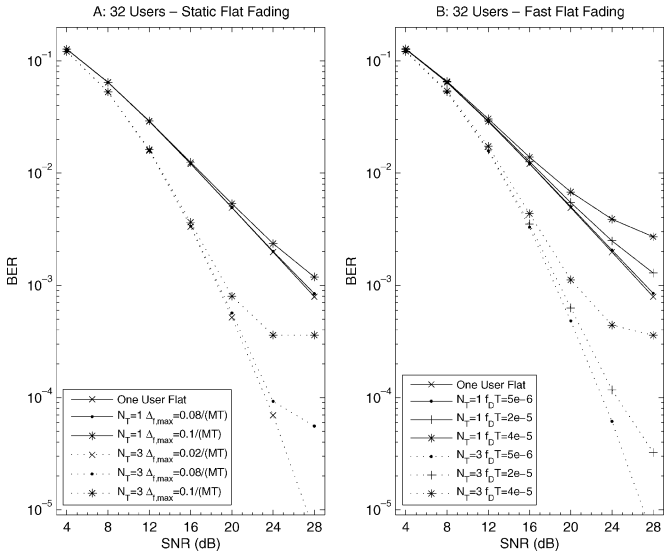

Fig. 8. Average BER performance of concatenated DMT-FMT with 32 asynchronous users with $\Delta_{\tau,\max} = 2T_0$ in quasi-static flat fading for different number of transmit antennas and values of maximum frequency offset (plot A). 32 asynchronous users with $\Delta_{\tau,\max} = 2T_0$ in flat fading with Jakes Doppler spectrum and different number of transmit antennas and values of normalized Doppler spread $f_D T$ (plot B).

starts to be visible when the maximum user' frequency offsets exceed the frequency guard. In Fig. 7, we compare the performance of a fully loaded system (solid curves) with a single-user system (dashed curves), where the user deploys the same number of FMT subchannels as in the fully loaded system. Note that the BER worsens only for the high SNRs although in the fully loaded system the users are asynchronous with $\Delta_{f,\max} = 0.08/(MT)$. To better understand the effect of the carrier frequency offset, in Fig. 8(a), we assume a quasi-static flat Rayleigh-fading channel with 32 asynchronous users (worst case scenario) that have a variable $\Delta_{f,\max}$. Fig. 8(a)

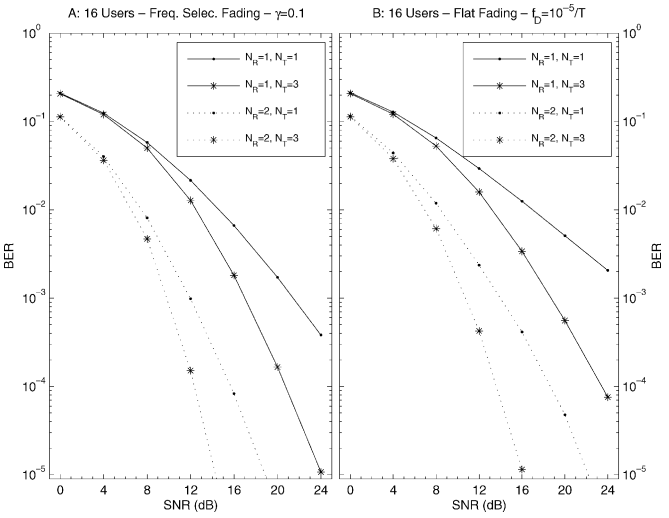

Fig. 9. Average BER performance of concatenated DMT-FMT for 16 asynchronous users in a fully loaded system with $\Delta_{\tau,\max} = 2T_0$ and $\Delta_{f,\max} = 0.02/(MT)$ for different number of transmit and receive antennas in frequency-selective fading with decay factor $\gamma = 0.1$ (plot A) and in flat fading with Doppler spread $f_D T = 10^{-5}$ (plot B).

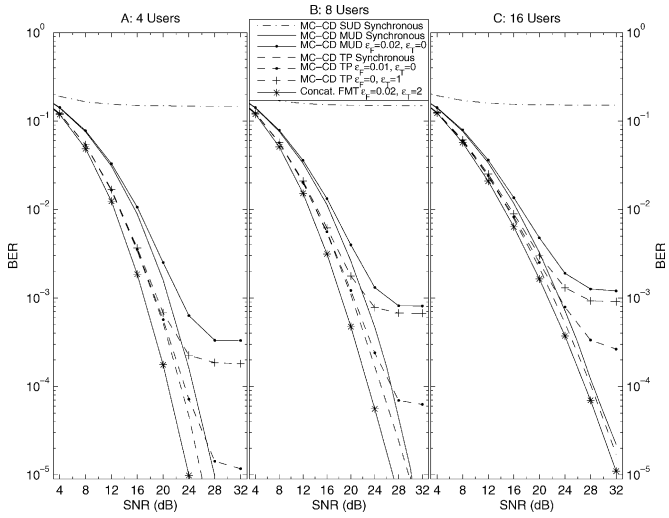

Fig. 10. Average BER performance of MC-CDMA (MC-CD), MC-CDMA with tone partitioning (MC-CD TP), and of the proposed concatenated DMT-FMT scheme (concatenated FMT) with one transmit-receive antenna. Frequency-selective fading with decay factor $\gamma = 0.1$, fully loaded system with synchronous or asynchronous users with $\Delta_{\tau,\max} = \varepsilon_T T_0$, and $\Delta_{f,\max} = \varepsilon_F/(MT)$ with $M = 32$.

shows that at $\mathrm{BER} = 10^{-3}$ the SNR gain is 8 dB with three transmit antennas compared with the single-antenna case. An error floor comes in at high SNRs for large frequency offsets. However, the ST-CP-DMT diversity scheme is capable of improving performance even when $\Delta_{f,\max}$ equals 10% of the FMT subcarrier spacing. Clearly, as explained in Section V, we always have the option of using larger frequency guards (at the expense of data rate). Further, the design should also take into account the presence of channel time variations. In principle, if the maximum Doppler is smaller than the frequency guards, and the coherence time is much larger than both the duration of the prototype pulse and of the duration of the ST-CP-DMT symbol, there is no loss of system orthogonality. In practice, it is not always possible to fulfill such conditions. Thus, to assess the effect of time-variant fading, we consider in Fig. 8(b) a system with 32 users that transmit over independent flat faded channels that have a Jakes' Doppler spectrum. The maximum normalized Doppler spread is equal to $f_D T = 5 \times 10^{-6}$, 2×10^{-5}, 4×10^{-5}. With the parameters in Table II and with a transmission bandwidth of $1/T = 10$ MHz, the Doppler spread equals 50, 200, and 400 Hz. The results in Fig. 8(b) show that the scheme is robust to channel time selectivity. Indeed, for $f_D T = 4 \times 10^{-5}$ some error floor is present, and it is primarily due to the loss of orthogonality in the outer DMT stage. With transmit diversity, we can counteract the detrimental effect of fast fading. Even for such a large Doppler, at $\mathrm{BER} = 10^{-3}$, the SNR gain with three transmit antennas is larger than 6.5 dB compared with the single antenna with static fading case.

Finally, in Fig. 9, we report a performance example that can be achieved when we use two receive antennas. We assume 16 asynchronous users over a frequency-selective channel with $\gamma = 0.1$ (Plot A) and over a flat fading channel with Doppler spread equal to $f_D T = 10^{-5}$ (Plot B). In both scenarios, the improvement is sensible when the number of transmit-receive antennas increases. With two receive antennas, at $\mathrm{BER} = 10^{-3}$, the SNR gain that can be achieved with three transmit antennas is about 2.5 dB in Fig. 9(a), and 3.5 dB in Fig. 9(b), compared with the single transmit antenna case.

C. Performance Comparison of Concatenated DMT-FMT With MC-CDMA

In Fig. 10, we compare the performance of the proposed concatenated DMT-FMT system with multicarrier CDMA (MC-CDMA) assuming a single transmit-receive antenna. MC-CDMA is essentially a DMT scheme, where all tones are assigned to all users and multiplexing is obtained by partitioning the codes among the users [15], [16]. Since the data symbols are spread over the whole tones (bandwidth) with a unique code, MC-CDMA can exploit the full frequency diversity. MC-CDMA has proved to be effective in the downlink [15]. In the uplink, it is severely affected by the MAI that is generated by both the independent frequency-selective channels and the users' asynchronism. Fig. 10 shows an example of the performance of MC-CDMA with 4, 8, and 16 users. MC-CDMA has 128 tones and a long cyclic prefix of length 72 to counteract the propagation delays. Walsh codes of length 128 are used. All spreading codes are assigned such that the data rate is identical for the various schemes herein evaluated. For MC-CDMA single-user detection (SUD) is not sufficient in the uplink even with synchronous users such that multiuser detection (MUD) becomes mandatory. Herein, we consider MMSE MUD [1], [29] with ideal channel knowledge. Although MC-CDMA has the potentiality of exploiting the full frequency diversity, its performance is limited by the MAI even with MUD and synchronous users. Further, the BER worsens with the users time/frequency asynchronism. To lower complexity and make the scheme more robust in the asynchronous channel, we also report the performance of MC-CDMA when we partition in a block fashion the tones across the users [5] (curves labeled with MC-CD TP). In this case, with simpler SUD the performance improves because tone partitioning reduces the

MAI. Nevertheless, the concatenated FMT scheme has the best performance in all cases here considered (from about 2 to 4 dB gain at $\mathrm{BER} = 10^{-4}$ over synchronous MC-CDMA), although the users have access to less frequency diversity resources as their number increases. Note that for the FMT scheme, we assume time/frequency offsets that are larger than the ones assumed for MC-CDMA. Spatial diversity gains can be obtained when multiple transmit antennas are used, as shown in the previous section. To obtain further diversity and interference averaging benefits, we can also use frequency hopping over the FMT subchannels with spreading along both the frequency and time direction as treated in [28]. Further improvements are expected with optimal maximum-likelihood detection (instead of simple one tap MMSE as here considered). Finally, the proposed scheme is robust to the near–far problem, and it allows to effectively implement synchronization and channel estimation exploiting the separability of multiple users signals in the frequency domain [23].

VII. Conclusion

We have presented an air-interface approach for next generation uplink wireless communications. It is based on the concatenation of an inner FMT modulator and an outer ST-CP-DMT modulator. Frequency and space diversity is exploited via DS data spreading across the DMT tones that fall within the FMT subchannels that are assigned to a given user. We have reported a detailed analysis to determine the conditions under which the multiuser multiple-antenna system orthogonalizes the asynchronous multiple-access channel. Numerical results show that the scheme is very robust to channel time/frequency selectivity and users' time/frequency offsets. Further, the ST-CP-DMT with DS spreading provides sensible performance gains. In particular, it allows to recover the diversity gain loss for the users that transmit at low rate and occupy a fraction of the overall spectrum.

In this paper, we have considered a simple single-user-based receiver. Increased performance (at the expense of complexity) can be obtained with a multiuser multichannel maximum *a posteriori* detector (or simplified iterative versions), as described in [6] in the event that significant ISI, ICI, and MAI components are present, e.g., when the frequency offsets exceed the frequency guard, the delay spread exceeds the one used for the system design, the Doppler spread is high. Although we do not discuss it in this paper, channel coding can also be added. A reasonable and popular choice is to use bit-interleaved codes [6], [15].

References

[1] S. Verdu, *Multiuser Detection*. Cambridge, U.K.: Cambridge Univ Press, 1998.

[2] Z. Wang and G. Giannakis, "Wireless multicarrier communications," *IEEE Signal Process. Mag.*, vol. 17, no. 3, pp. 29–48, May 2000.

[3] C. Yui, R. Cheng, K. Ben Letaief, and R. Murch, "Multiuser OFDM with adaptive subcarrier, bit, and power allocation," *IEEE J. Sel. Areas Commun.*, pp. 1747–1758, Oct. 1999.

[4] A. Tonello, N. Laurenti, and S. Pupolin, "Analysis of the uplink of an asynchronous DMT OFDMA system impaired by time offsets, frequency offsets, and multi-path fading," in *Proc. IEEE Veh. Technol. Conf. (Fall)*, Boston, MA, Sep. 2000, pp. 1094–1099.

[5] S. Kaiser and W. Krzymien, "Performance effects of the uplink asynchronism is a spread spectrum multi-carrier multiple access system," *Eur. Trans. Telec.*, pp. 399–406, Jul.-Aug. 1999.

[6] A. Tonello, "Asynchronous multicarrier multiple access: Optimal and suboptimal detection and decoding," *Bell Labs Tech. J.*, vol. 7, no. 3, pp. 191–217, 2003.

[7] A. Tonello and S. Pupolin, "Discrete multi-tone and filtered multi-tone architectures for broadband asynchronous multi-user communications," in *Proc. Wireless Pers. Multimedia Commun.*, Aalborg, Denmark, Sep. 2001, pp. 461–466.

[8] ——, "Performance of single user detectors in multitone multiple access asynchronous communications," in *Proc. of IEEE Veh. Technol. Conf. (Spring)*, Birmingham, May 2002, pp. 199–203.

[9] G. Cherubini, E. Eleftheriou, S. Ölçer, and J. Cioffi, "Filter bank modulation techniques for very high-speed digital subscriber lines," *IEEE Commun. Mag.*, vol. 38, no. 5, pp. 98–104, May 2000.

[10] G. Cherubini, E. Eleftheriou, and S. Ölçer, "Filtered multitone modulation for very high-speed digital subscribe lines," *IEEE J. Sel. Areas Commun.*, vol. 20, no. 5, pp. 1016–1028, Jun. 2002.

[11] N. Benvenuto, S. Tomasin, and L. Tomba, "Equalization methods in OFDM and FMT systems for broadband wireless communications," *IEEE Trans. Commun.*, vol. 50, no. 9, pp. 1413–1418, Sep. 2002.

[12] A. Tonello, "Performance limits for filtered multitone modulation in fading channels," *IEEE Trans. Wireless Commun.*, vol. 4, no. 5, pp. 2121–2135, Sep. 2005.

[13] A. Dammann, R. Raulefs, G. Auer, and G. Bauch, "Comparison of space-time block coding and cyclic delay diversity for broadband mobile radio air interface," in *Proc. Wireless Pers. Multimedia Commun. 2003*, vol. 2, Oct. 2003, pp. 411–415.

[14] A. Tonello, "Orthogonal space-time discrete multitone and space-time filtered multitone coded architectures," in *Proc. IEEE Veh. Technol. Conf. (Spring)*, vol. 2, Milan, Italy, May 2004, pp. 713–717.

[15] S. Kaiser, "OFDM code division multiplexing in fading channels," *IEEE Trans. Commun.*, vol. 50, no. 8, pp. 1266–1273, Aug. 2002.

[16] L. Tomba and W. A. Krzymien, "Effect of carrier phase noise and frequency offset on the performance of multicarrier CDMA systems," in *Proc. IEEE Int. Conf. Commun.*, Dallas, TX, Jun. 1996, pp. 1513–1517.

[17] V. Tarokh, N. Seshadri, and A. R. Calderbank, "Space-time codes for high data rate wireless communication: Performance criterion and code construction," *IEEE Trans. Inf. Theory*, vol. 44, no. 2, pp. 744–765, Mar. 1998.

[18] G. Bauch and J. S. Malik, "Orthogonal frequency division multiple access with cyclic delay diversity," in *Proc. IEEE-ITG Worshop Smart Antennas*, Munich, Germany, Mar. 18–19, 2004.

[19] J. Winters, "The diversity gain of transmit diversity in wireless systems with Rayleigh fading," *IEEE Trans. Veh. Technol.*, vol. 47, no. 1, pp. 119–123, Feb. 1998.

[20] Y. G. Li, J. C. Chuang, and N. R. Sollenberger, "Transmitter diversity for OFDM systems and its impact on high-rate data wireless networks," *IEEE J. Sel. Areas Commun.*, vol. 17, no. 7, pp. 1233–1243, Jul. 1999.

[21] I. Lee, A. M. Chan, and C.-E. W. Sundberg, "Space-time bit-interleaved coded modulation for OFDM systems in wireless LAN applications," in *Proc. IEEE Int. Conf. Commun.*, May 2003, pp. 3413–3417.

[22] J. Liu and J. Li, "MIMO system with backward compatibility for OFDM based WLANs," *EURASIP J. Appl. Signal Process.*, vol. 2004, no. 5, pp. 696–706, 2004.

[23] A. Tonello and F. Pecile, "Synchronization algorithms for multiuser filtered multitone (FMT) systems," in *Proc. IEEE Veh. Technol. Conf. (Spring)*, Stockholm, Sweden, May 2005, pp. 1778–1782.

[24] A. Tonello, "MIMO MAP equalization and turbo decoding in interleaved space-time coded systems," *IEEE Trans. Commun.*, vol. 51, no. 2, pp. 155–160, Feb. 2003.

[25] M. V. Clark, "Adaptive frequency-domain equalization and diversity combining for broadband wireless communications," *IEEE J. Sel. Areas Commun.*, vol. 16, no. 8, pp. 1385–1395, Oct. 1998.

[26] J. van de Beek *et al.*, "A time and frequency synchronization scheme for multiuser OFDM," *IEEE J. Sel. Areas Commun.*, vol. 17, no. 11, pp. 1900–1914, Nov. 1999.

[27] G. L. Stuber, *Principles of Mobile Communications*. Norwell, MA: Kluwer, 1996.

[28] A. Tonello and A. Assalini, "An asynchronous multitone multiuser air interface for high-speed uplink communications," in *Proc. IEEE Veh. Technol. Conf. (Fall)*, vol. 4, Orlando, FL, Sep. 2003, pp. 2267–2271.

[29] S. L. Miller and B. J. Rainbolt, "MMSE detection of multicarrier CDMA," *IEEE J. Sel. Areas Commun.*, vol. 18, no. 11, pp. 2356–2362, Nov. 2000.

Andrea M. Tonello (S'00–M'02) received the Doctor of Engineering degree in electronics (*cum laude*) and the Doctor of Research degree in electronics and telecommunications from the University of Padova, Padova, Italy, in 1996 and 2002, respectively.

In 1997, he was a Member of Technical Staff, Bell Laboratories, Lucent Technologies, Holmdel, NJ, where he worked on the development of baseband algorithms for cellular handsets, and then within the Philips/Lucent Consumer Products Division, Piscataway, NJ. From September 1997 to December 2002, he was with the Bell Laboratories Advanced Wireless Technology Laboratory, Whippany, NJ. He was promoted in 2002 to Technical Manager, and was appointed Managing Director of Bell Laboratories Italy. He has been on leave from his position for part of the period covered from September 1999 to March 2002, while at the University of Padova. In January 2003, he joined the Dipartimento di Ingegneria Elettrica, Gestionale e Meccanica (DIEGM), University of Udine, Udine, Italy, where he is currently an Assistant Professor (*ricercatore*). He is the author of several papers and patents. He has been involved in the standardization activity for the evolution of the IS-136 TDMA technology within UWCC/TIA. His research interests include wireless and powerline communications.

Dr. Tonello received a Lucent Bell Laboratories Recognition of Excellence Award for his work on enhanced receiver techniques. He is a member of the IEEE Communications Society Broadband Over Powerline Technical Subcommittee.